Copper, zinc superoxide dismutase of Curcuma aromatica is a kinetically stable protein

ARTICLE *in* PROCESS BIOCHEMISTRY · APRIL 2014

Impact Factor: 2.52 · DOI: 10.1016/j.procbio.2014.04.010

Process Biochemistry 49 (2014) 1288–1296

Contents lists available at ScienceDirect

Process Biochemistry

journal homepage: www.elsevier.com/locate/procbio

Copper, zinc superoxide dismutase of *Curcuma aromatica* is a kinetically stable protein

Arun Kumar[1], Anish Kaachra, Shruti Bhardwaj, Sanjay Kumar*

Biotechnology Division, CSIR-Institute of Himalayan Bioresource Technology, Palampur 176 061, Himachal Pradesh, India

ARTICLE INFO

Article history:
Received 28 November 2013
Received in revised form 5 April 2014
Accepted 7 April 2014
Available online 19 April 2014

Keywords:
Superoxide dismutase
Autoclave stable
Thermal inactivation
Trypsin
Sodium dodecyl sulfate
Kinetic stability

ABSTRACT

This study details on cloning and characterization of *Cu,Zn superoxide dismutase* (*Ca–Cu,Zn SOD*) from a medicinally important plant species *Curcuma aromatica*. *Ca–Cu,Zn SOD* was 692 bp with an open reading frame of 459 bp. Expression of the gene in *Escherichia coli* cells followed by purification yielded the enzyme with K_m of 0.047 ± 0.008 μM and V_{max} of 1250 ± 24 units/mg of protein. The enzyme functioned (i) across a temperature range of −10 to +80 °C with temperature optima at 20 °C; and (ii) at pH range of 6–9 with optimum activity at pH 7.8. Ca–Cu,Zn SOD retained 50% of the maximum activity after autoclaving, and was stable at a wide storage pH ranging from 3 to 10. The enzyme tolerated varying concentrations of denaturating agent, reductants, inhibitors, trypsin, was fairly resistant to inactivation at 80 °C for 180 min (k_d, 6.54 ± 0.17 × 10^{-3} min^{-1}; $t_{1/2}$, 106.07 ± 2.68 min), and had midpoint of thermal transition (T_m) of 70.45 °C. The results suggested Ca–Cu,Zn SOD to be a kinetically stable protein that could be used for various industrial applications.

1. Introduction

One of the immediate responses of living organisms to environmental stress is the enhanced production and accumulation of reactive oxygen species (ROS), which include singlet oxygen ($^1O_2$), hydrogen peroxide (H_2O_2), superoxide radical ($O_2^{-\bullet}$), hydroxyl radical ($OH^\bullet$), hydroperoxyl radical/perhydroxyl ($HO_2^\bullet$), alkoxy radical ($RO^\bullet$), peroxy radical ($ROO^\bullet$) and excited carbonyl (RO^*) [1–5]. ROS are required for several physiological functions of the aerobes and have important roles in cellular metabolism [6]. Also, ROS attack virtually all macromolecules leading to serious damage in cellular components, DNA lesions, mutations, and often result in irreparable metabolic dysfunction, and cell death [4]. Overwhelming production of ROS coupled with insufficient scavenging by enzymatic and non-enzymatic routes lead to detrimental effects in varied organisms [7,8].

Superoxide dismutase (SOD) (EC 1.15.1.1) has an important role in combating $O_2^{-\bullet}$ mediated cellular damage and constitutes the first line of enzymatic defense within a cell by catalyzing the dismutation of $O_2^{-\bullet}$ to O_2 and H_2O_2 [9,10]. Since phospholipids membranes are impermeable to charged O_2 molecules, scavenging mechanisms including SODs ought to be present in various cellular compartments to protect against $O_2^{-\bullet}$ mediated toxicity [11]. Based on the metal co-factor used by the enzyme, SODs are classified into four groups: iron SOD (Fe SOD), manganese SOD (Mn SOD), nickel SOD (Ni SOD) and copper, zinc SOD (Cu,Zn SOD) [7,12,13]. These are localized in different compartments of the cell: Fe SOD is localized in chloroplast, Mn SOD is present in the mitochondria and peroxisome, Ni SOD is present in the cytosol, whereas Cu,Zn SOD is present in the chloroplast, cytosol, and possibly in the extracellular space [7,12].

Diverse organeller distribution of Cu,Zn SOD and its association with stress tolerance is one of the likely reasons for large number of studies on the enzyme [9,14–18]. From industrial perspective, SOD has a huge market potential and finds applications in food, pharmaceutical and cosmetic industries [7,8,11,14–18]. Therefore, SODs with a wide range of kinetic stability are required for targeted or specialized applications.

Curcuma aromatica (wild turmeric, family Zingiberaceae) is a perennial herb native to southern India and is also present across an altitude of 700–2500 m amsl in Himalayas in India and Nepal, and in Sri Lanka. The species is reported to have anti-inflammatory, antioxidant, antimelanogenic, hepatoprotective, anti-cancer properties [19]. It is also proposed to have therapeutic potential for the prevention of hyperglycemia-associated diabetic complications

* Corresponding author. Tel.: +91 1894 233339; fax: +91 1894 230433.
E-mail addresses: sanjaykumar@ihbt.res.in, sanjayplp@rediffmail.com (S. Kumar).
[1] Present address: Plant Science Department, McGill University, Sainte-Anne-de-Bellevue, Quebec, Canada H9X3V9.

http://dx.doi.org/10.1016/j.procbio.2014.04.010
1359-5113/

Table 1
Primer sequences and PCR conditions used for amplification of partial *Ca–Cu,Zn SOD*. FP, forward primer; RP, reverse primer.

Primer sequence (5′-3′)[a]	PCR conditions
FP: CAGGAAGGAGATGGYCCAACM	94 °C, 3 min; 35 cycles: 94 °C, 30 s; 55 °C, 40 s; 72 °C, 1 min
RP: YTGAARRCCRATVCCACAAGC	Final extension at 72 °C, 7 min

[a] Y, C/T; M, A/C; R, A/G; V, G/A/C.

[20]. The antioxidant properties associated with *C. aromatica* has been postulated to play a role in the suppression of ROS-induced tissue injury [20]. Toluene extract of *C. aromatica* exhibited free radical scavenging activity in assays conducted both in *in vivo* as well as *in vitro* models [21].

Incidentally, during its growth cycle, *C. aromatica* experiences several abiotic stress conditions including high temperature and drought, which is likely to cause oxidative stress. Hence the species is expected to harbor antioxidant machinery including SOD to confer protection under the stressful environment [22]. Objective of the present work was to clone and functionally characterize Cu,Zn SOD from *C. aromatica*.

2. Materials and methods

Leaf tissues of *C. aromatica* Salisb. were collected in the morning at 10:00 am from the experimental farm of the Institute of Himalayan Bioresource Technology at Palampur (latitude 32°06′; longitude 76°33′; 1300 m amsl; Distt. Kangra, HP, India), dipped in liquid nitrogen and stored in −80 °C till further use.

2.1. Cloning of Cu,Zn SOD from C. aromatica

RNA was isolated following the method of Ghawana et al. [23] and treated with DNase I (amplification grade, Invitrogen, USA) to remove contaminating genomic DNA. First strand cDNA of DNA-free RNA was synthesized using total RNA (2 μg) in the presence of 0.5 μg oligo(dT) 12–18 primer (Invitrogen, USA) and 400 U of Superscript reverse transcriptase [(RT); Invitrogen, USA] following manufacturer's instructions. Resulting cDNA (1 μl per reaction of 25 μl) was used for PCR using degenerate primers (Table 1) and 1 U *Taq* DNA polymerase (Qiagen, Germany) on a GeneAmp 9700 cycler (Applied Biosystems, USA) as per the cycling conditions detailed in Table 1. Degenerate primers (Table 1) were designed using the sequences of *Cu,Zn SODs* retrieved from NCBI database and aligned using multiple sequence alignment by CLUSTALW software program (http://align.genome.jp). Highly conserved regions were used to design primers that also covered catalytic domain and cysteines involved in disulfide linkage.

PCR-amplified fragments were extracted from the gel and ligated into pGEM®-T Easy vector (Promega, USA). The sequence information was used for designing primers (Table 2) for rapid amplification of cDNA ends (RACE). The cDNA was synthesized using the DNA-free RNA isolated from leaf tissue using SMART™ RACE cDNA amplification Kit (BD Biosciences, Clontech, USA) as per the manufacturer's instructions. PCR was performed using the cycling conditions as defined in Table 2. Amplicons were cloned in pGEM®-T Easy vector, and sequenced. The resulting 5′ and 3′ sequences were aligned using NCBI BLAST align software (http://www.ncbi.nlm.nih.gov/). Subsequently, full-length cDNA clones were amplified using the primers designed from start and stop codons (Table 2), cloned in pQE-30 UA expression vector (Qiagen, Germany) and transformed in competent *E. coli* strain M15.

2.2. Bioinformatic analyses

Sequences were analyzed by BLAST algorithm at NCBI database (http://www.ncbi.nlm.nih.gov/). Homology search was conducted using BLASTN and BLASTX algorithm (http://www.ncbi.nlm.nih.gov/). Deduced amino acid sequence was used to analyze protein families and domains using the tools available at PROSITE database at ExPASy Proteomics Server (http://ca.expasy.org/), SMART (http://smart.embl-heidelberg.de/) and NCBI conserved domain search (http://www.ncbi.nlm.nih.gov/structure/cdd/). SOPMA (http://npsa-pbil.ibcp.fr) was used for secondary structure prediction of the deduced protein. Homology modeling for prediction of three dimensional (3-D) structure was done using ExPASy proteomic server (http://beta.swissmodel.expasy.org/workspace/index.php?func=modelling_beta1).

QMEAN4 score was used for assessing the quality of predicted 3-D structures. The QMEAN4 score [24] is a composite score consisting of a linear combination of four statistical potential terms *viz.* Cβ interaction energy, all-atom pairwise energy, solvation energy, and torsion angle energy (estimated model reliability between 0 and 1) [25]. The model's QMEAN score was compared to the scores obtained for experimental structures of similar size (model size ± 10%) and a *Z*-score was calculated. A *Z*-score is a score which is normalized to mean 0 and standard deviation 1. Higher values of *Z*-score represent good quality models. Thus the QMEAN *Z*-score directly indicated the difference in standard deviations between the model's QMEAN score and expected values for experimental structures. MEGA5 software (http://www.megasoftware.net) was used for phylogenetic analysis [26]. Neighbor joining method was used for analysis and the bootstrap was calculated using 1000 replications.

2.3. Expression and purification of Ca–Cu,Zn SOD

E. coli harboring *Ca–Cu,Zn SOD* was grown in 1000 ml of Luria Broth containing 100 μg ml^{-1} ampicillin and 25 μg ml^{-1} kanamycin at 37 °C in an incubator shaker (shaking, 250 rpm). Expression of *Ca–Cu,Zn SOD* was induced by addition of 1 mM of isopropyl β-D-1-thiogalactopyranoside (IPTG) when culture grew to an absorbance of 0.6 at 600 nm. $CuSO_4$ and $ZnSO_4$ were added to a final concentration of 100 ppm and 2 ppm, respectively [17]. After 5 h of IPTG addition, cells were harvested by centrifugation at 4000 × *g* at 4 °C for 20 min. Pellets were resuspended in 50 ml of lysis buffer (50 mM NaH_2PO_4, 300 mM NaCl and 10 mM imidazole; pH 8.0) and lysozyme was added to a final concentration of 1 mg/ml. Resuspended cells were incubated on ice for 30 min. The cell suspension was sonicated using a Misonix sonicator 3000 (Misonix Inc., USA) equipped with a microtip (four cycles where each cycle was a 10 s burst of sonication, followed by a 5 s pause in between), and the lysate obtained was cleared by centrifugation (12,000 × *g* and 4 °C for 20 min). Supernatant was loaded onto nickel–nitrilotriacitic acid (Ni–NTA) column (Qiagen, Germany), washed with wash buffer (50 mM NaH_2PO_4, 300 mM NaCl and 20 mM imidazole; pH 8.0), and induced proteins were eluted with elution buffer (50 mM NaH_2PO_4, 300 mM NaCl and 250 mM imidazole; pH 8.0). The purified protein was extensively dialysed against 50 mM phosphate buffer (pH, 7.8), and concentrated by using Amicon Ultra 15 ml centrifugal, 10 kDa-cutoff filter (Millipore, USA).

2.4. SDS-PAGE analysis of expressed proteins

Protein was denatured by boiling the solution for 10 min in the presence of denaturing sample loading buffer [62.5 mM Tris–Cl (pH, 6.8), 10% glycerol, 2.5% SDS, 0.002% bromophenol blue, and 0.7135 M 2-mercaptoethanol (2-ME)]. Samples were

Table 2
Primer sequences and PCR conditions used in RACE reactions and amplification of coding sequence (CDS) of *Cu,Zn SOD* of *Curcuma aromatica*.

Primers sequences (5′–3′)[a]	PCR conditions
GSP1: 5′-GTAGGAAGTGAGACTGTTATTGACAA-3′ NGSP1: 5′-TGTCAATTGGGTTGAGAGTAAC-3′ GSP2: 5′-CACCACTTTTGATCTTCCTTACAAT-3′ NGSP2: 5′-CCTACATATCAAATGAAGCAACTCA-3′	Primary PCR 5 cycles: 94 °C, 30 s; 72 °C, 3 min; followed by 5 cycles: 94 °C, 30 s; 70 °C, 30 s; 72 °C, 3 min; and 30 cycles: 94 °C, 30 s; 68 °C, 30 s; 72 °C, 3 min; Final extension at 72 °C, 7 min
Universal primer mix (UPM): supplied by the manufacturer 5′-CTAATACGACTCACTATAGGGCAAGCAGTGGTATCAACGCAGAGT-3′ 5′-CTAATACGACTCACTATAGGGC-3′	
Nested universal primer (NUP): supplied by the manufacturer 5′-AAGCAGTGGTATCAACGCAGAGT-3′	Nested PCR 30 cycles: 94 °C, 30 s; 68 °C, 30 s; 72 °C, 3 min; Final extension at 72 °C, 7 min
CDSF: 5′-ATGGTGAAGGCTGTTGCTGTCCT-3′	1 cycle: 95 °C, 3 min; 30 cycles: 94 °C, 30 s; 54 °C, 30 s; 72 °C, 2 min. Final extension at 72 °C, 7 min
CDSR: 5′-TCATCCTTGAAGGCCAATAATACC-3′	

[a] GSP1, gene specific primer for 3′-RACE; NGSP1, nested gene specific primer for 3′-RACE; GSP2, gene specific primer for 5′-RACE; NGSP2, nested gene specific primer for 5′-RACE. CDSF, forward primer for amplification of CDS; CDSR, reverse primer for amplification of CDS.

chilled on ice for 5 min followed by centrifugation at 13,000 × *g*. The supernatant was separated and loaded on to 15% SDS-PAGE [32]. Proteins were run at 25 mA using 1× Tris–glycine (containing 0.1% SDS) as running buffer. When the samples reached the resolving gel, current was increased to 35 mA till the end of run. The gel was stained by silver staining [27].

2.5. Determination of SOD activity

The following methods were used for assaying SOD activity spectrophotometrically as well for activity staining on the polyacrylamide gel. Enzyme was assayed by measuring inhibition in photoreduction of nitroblue tetrazolium (NBT) by SOD [9]. Reaction medium contained 50 mM phosphate buffer (pH, 7.8), 5.7×10^{-5} M NBT, 9.9×10^{-3} M methionine, 1.17×10^{-6} M riboflavin and 0.025% Triton X-100 in a final volume of 200 μl. SOD was assayed on a microtitre plate by exposing the reaction to white light for 10 min. A control reaction was always performed wherein all the steps and components were the same as described above except that protein sample was replaced with equal volume of 50 mM potassium phosphate buffer (pH 7.8). For assaying at sub-zero temperatures, 50% glycerol (final concentration) was added in the reaction mixture to avoid freezing and the assay was carried out by placing a 96-well plate inside a −20 °C freezer. Absorbance was recorded at 560 nm using a spectrophotometer having a microplate reader (Synergy HT, with Gen5 controlling software, Bioteck, USA). Activity of SOD was expressed as units per mg protein [9].

Activity of SOD on the gel was visualized by activity staining as described previously [28]. Gel was incubated in 50 mM phosphate buffer (pH 7.8) containing 2.5 mM NBT and kept in dark in a cold room. After 30 min, NBT solution was decanted and the gel was incubated for 20 min in 50 mM phosphate buffer (pH 7.8) containing 1.5 μM riboflavin. Following this, the riboflavin solution was decanted off and the gel was exposed to light. This generated dark blue color in the entire gel except in the region of SOD protein band.

2.6. Determination of kinetic parameters of Ca–Cu,Zn SOD

The effect of varying concentrations of riboflavin was studied as described previously [29]. Separate reaction mix with varying concentrations of riboflavin (0.00, 0.0625, 0.075, 0.125, 0.25, 0.50, and 0.75 μM) were prepared and Ca–Cu,Zn SOD was assayed using 1 μg protein for each reaction in triplicates as described in previous section. Separate control reactions were performed wherein in place of the enzyme, 50 mM phosphate buffer (pH, 7.8) was added to the reaction. Specific activity of the enzyme was calculated to determine the Michaelis–Menten kinetics. Double reciprocal/Lineweaver–Burk plot was prepared by plotting the reciprocal of the substrate concentration [S] against inverse of specific activity of the enzyme [1/V]. Maximum enzyme velocity (V_{max}) and Michaelis constant (K_m, the substrate concentration at which enzyme shows half of V_{max}) were calculated by using the equation from the resulting slope of the graph. The slope, *y* intercept, and *x* intercept represents K_m/V_{max}, $1/V_{max}$, and $-1/K_M$, respectively [30].

2.7. Determination of pH optima

SOD was assayed [9] either in phosphate or carbonate-bicarbonate buffer depending upon the assay pH: 50 mM phosphate buffer was used for pH 6.0, 7.0, 7.5, 7.8; 50 mM carbonate–bicarbonate buffer was used for pH, 9.0; the two different buffers were used due to difference in their pK_a values. Separate controls reactions were set up in triplicates wherein all the components were the same except that equal amount of buffer was added to the reaction medium in place of the enzyme. Enzyme activity was calculated as percent inhibition in reduction of NBT with respect to the control at respective pH.

2.8. Effect of storage pH on enzyme stability

The stability of enzyme as a function of pH was determined at 37 °C by quantifying residual activity after 2 and 24 h of incubation at various pH. Enzyme was desalted and concentrated by using Amicon Microcon Centrifugal Filter Devices (Microcon YM-3; Millipore, USA) as per manufacturer's instructions.

Three times volume of buffer of different pH values was added to the desalted Ca–Cu,Zn SOD as follows: 50 mM glycine–HCl (pH 3.0), 50 mM acetate buffer (pH 4.0, 5.0), 50 mM potassium phosphate buffer (pH 6.0, 7.0, 8.0), or 50 mM carbonate–bicarbonate buffer (pH 9.0, 10.0). After 2 and 24 h of incubation, SOD was blended with 50 mM phosphate buffer (pH, 7.8) in the ratio of 1:10 and incubated for 30 min [31]. SOD was assayed under standard assay conditions in triplicates. Control reactions in triplicates were also carried out for each pH value, wherein SOD was incubated for specified time period in phosphate buffer. Percent relative activity with respect to the maximum activity was plotted against each pH value.

2.9. Effect of denaturating agent, reducing agents and inhibitors on the activity of Ca–Cu,Zn SOD

Effect of denaturating agent (guanidinium hydrochloride, GuHCl), reducing agents [dithiothreitol (DTT); and 2-ME], and inhibitors [ethylenediaminetetraacetic acid (EDTA), and hydrogen peroxide (H_2O_2)] was investigated on the activity of Ca–Cu,Zn SOD. The enzyme containing each of the above compounds in a defined concentration was incubated in 50 mM phosphate buffer (pH, 7.8) at 37 °C for 1 h. Control reactions were always performed in the presence of above compounds.

2.10. Thermal inactivation assay

Thermal inactivation kinetics of Ca–Cu,Zn SOD was studied as described previously [9] with slight modifications. Purified enzyme (0.05 mg/ml) was aliquoted in 10 separate 0.2 ml PCR tubes. All aliquots except zero min control were heated in a PCR block maintained at 80 °C for defined time intervals. Aliquots were removed every 20 min till 180 min and stored on ice. All the aliquots were evaluated for SOD activity under standard assay conditions and the activity data was fit into zero-order (residual activity *versus* time), first-order (natural logarithm of residual activity *versus* time), and second-order (reciprocal of residual activity *versus* time) thermal inactivation kinetics. The rate constant k_d (min^{-1}) and the half-time of thermal inactivation ($t_{1/2}$) for first-order thermal inactivation was determined from the slope of the inactivation time course [9]. Accordingly, equations, $\ln(A_t/A_0) = -k_d \times t$ and $t_{1/2} = \ln(2)/k_d$ were used for various calculations. Where A_t is the residual activity that remains after heating the enzyme for time *t*, and A_0 is the initial enzyme activity before heating.

2.11. Measurements of protein stability by thermal unfolding

Differential scanning calorimetry (DSC) measurement for characterization of thermal denaturation of protein was performed on a MicroCal VP-DSC calorimeter (volume of the cell = 0.523 ml; MicroCal/GE Healthcare, Northampton, MA, USA) using 0.044 mM Ca–Cu,Zn SOD in phosphate buffer (100 mM, pH 7.4); reference cell had phosphate buffer (100 mM, pH 7.4) only. The samples were heated from 10 °C to 110 °C at a heating rate of 90 °C/h. Various parameters were set as follows: the prescan for 10 min, the filtering period was 30 s, and the feedback mode/gain was set to none. A blank measurement with phosphate buffer in both the compartments served as baseline. Protein and buffer were degassed for 30 min using Thermovac to avoid formation of air bubbles. The midpoint of a thermal transition (T_m) was obtained by analyzing the data using Origin 7 software supplied by the manufacturer.

2.12. Limited trypsin proteolysis

Ca–Cu,Zn SOD was blended with trypsin in a ratio of 1:20 (w/w) in 50 mM phosphate buffer (pH 7.8) in a microcentrifuge tube and incubated for defined time intervals in a water bath maintained at 37 °C [9]. Control reactions were also performed under identical conditions wherein 50 mM phosphate buffer (pH 7.8) was added in place of trypsin. Aliquots were removed at defined time intervals and evaluated for protein integrity by loading equal quantity of protein (1 μg) on 15% SDS-PAGE. Enzyme was evaluated for SOD activity on 10% native-PAGE by loading 300 ng each of control and trypsin treated samples, and by spectrophotometric assay as well. The Ca–Cu,Zn SOD sequence was also subjected to *in silico* analysis on PeptideCutter cutter software (http://web.expasy.org/peptide_cutter/) to evaluate the number of possible trypsin cleavage sites along the polypeptide backbone.

2.13. Resistance to sodium dodecyl sulfate (SDS) binding

Resistance of the enzyme to SDS-binding was evaluated by comparing the migration of boiled and unboiled protein on SDS-PAGE as described previously [32]. Equal quantity (1 μg) of the enzyme was either unboiled or boiled for 10 min in the sample loading buffer [62.5 mM Tris–Cl (pH, 6.8), 10% glycerol, 2.5% SDS, and 0.002% bromophenol blue]. The buffer was devoid of 2-ME, but had SDS [32,33]. Enzyme was loaded on 15% SDS-PAGE followed by silver staining to visualize the protein.

3. Results

3.1. Cloning of SOD

Degenerate primers designed in the present work (Table 1) amplified an amplicon of 387 bp (Supplementary Fig. 1), which upon sequencing was confirmed to be of *Cu,Zn SOD*. RACE yielded a 5′ amplicon of 900 bp and a 3′ amplicon of 380 bp from *C. aromatica* (Supplementary Fig. 2a and b). Full-length sequence of *Ca–Cu,Zn SOD* (692 bp) was obtained by aligning 5′ and 3′-RACE sequences. The full-length *Ca–Cu,Zn SOD* had an open reading frame (ORF) of 459 bp (Supplementary Fig. 2c) with start codon ATG at position 91 and a stop codon TGA at position 547 of the gene. The gene consisted of 5'-UTR of 91 bp, and 3′-UTR of 142 bp with a poly A^+ tail of 28 bp (Supplementary Fig. 3). The sequence was submitted to NCBI gene databank vide accession number FJ589638.

ORF of *Ca%3Fndash;Cu,Zn SOD* encoded 152 amino acids with calculated molecular mass of 15.18 kDa and a pI of 5.93. Ca–Cu,Zn SOD consisted of two highly conserved Cu,Zn SOD signatures. Signature

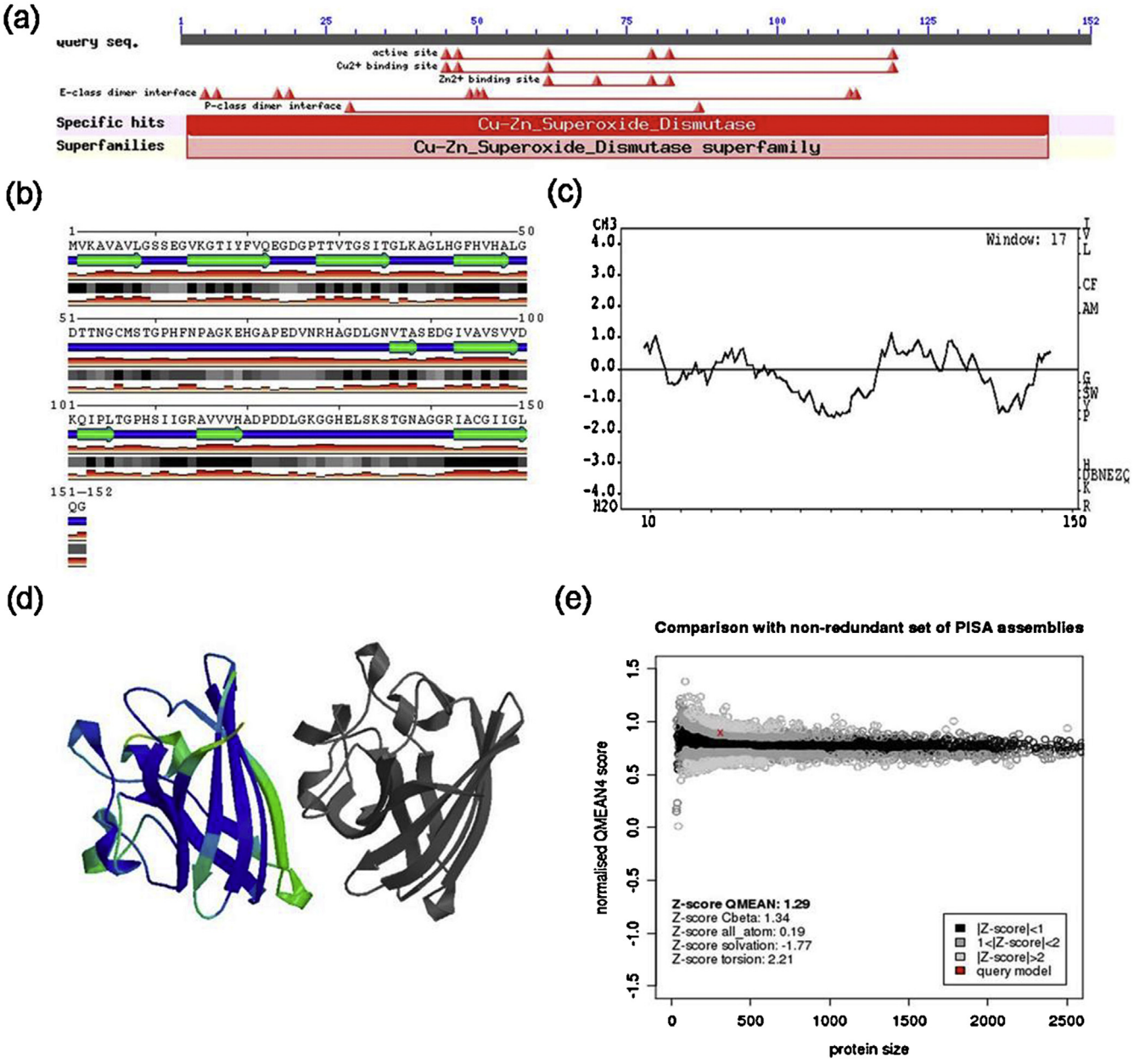

Fig. 1. Structural analysis of Ca–Cu,Zn SOD: (a) catalytic domain prediction by NCBI Conserved Domain Database Search; (b) secondary structure prediction; extended strand, and random coil are indicated in green and blue, respectively; (c) hydropathy plot; (d) predicted 3-D structure of Ca–Cu,Zn SOD using swiss model; (e) comparison of predicted structure with non-redundant PISA (protein interactions, surfaces and assemblies) assemblies. The area built by the circles colored in different shades of gray in the plot on the left hand side represents the QMEAN scores of the reference structures from the PDB. (For interpretation of the references to color in this figure legend, the reader is referred to the web version of the article.)

1 with a consensus of [GA] – [IMFAT] – H – [LIVF] – H – {S} – x – [GP] – [SDG] – x – [STAGDE] spanned amino acids Gly-43 to Thr-53. Consensus for Cu,Zn SOD signature 2 was G – [GNHD] – [SGA] – [GR] – x – R – x – [SGAWRV] – C – x(2) – [IV] that spanned from amino acids Gly-137 to Ile-148 (Supplementary Fig. 4). The amino acid residues important in coordinating copper (His-45, His-47, His-62, and His-119), and zinc (His-62, His-70, His-79, and Asp-82) were conserved. Also, the two cysteines (Cys-56 and Cys-145) that formed a single disulfide bond were conserved (Supplementary Fig. 4).

Ca–Cu,Zn SOD shared similarities with Cu,Zn SOD from *Bambusa oldhamii* (Bo-Cu,Zn SOD; 91%), *Pleioblastus fortunei* (Pf-Cu,Zn SOD; 90%), *Neosinocalamus affinis* (Na-Cu,Zn SOD; 89%), *Malus xiaojinensis* (Mx-Cu,Zn SOD; 88%), *Gossypium hirsutum* (Gh-Cu,Zn SOD; 86%), *Olea europaea* (Oe-Cu,Zn SOD; 85%), and *Melastoma malabathricum* (Ma-Cu,Zn SOD; 86%) (Supplementary Fig. 4). The conserved domain search of Ca–Cu,Zn SOD at NCBI showed that the amino acid sequence contained conserved domains important for catalytic activity of Ca–Cu,Zn SOD (Fig. 1a). SOPMA analysis showed that deduced Ca–Cu,Zn SOD was composed of alpha helices (5.26%) and random coils (53.29%) joined by extended strands (33.55%) and β-turns (7.89%) (Fig. 1b).

Hydropathy plot generated using Kyte and Doolittle algorithm at window size of 17 indicated that Ca–Cu,Zn SOD is a cytosolic protein with no transmembrane domain (Fig. 1c). The predicted 3-D model of the Ca–Cu,Zn SOD using target 2q2lA showed 85.526% sequence identity and *E*-value of $8.96842e^{-58}$. Model was successfully built as dimer with a QMEAN *Z*-score of 1.29 (Fig. 1d and e).

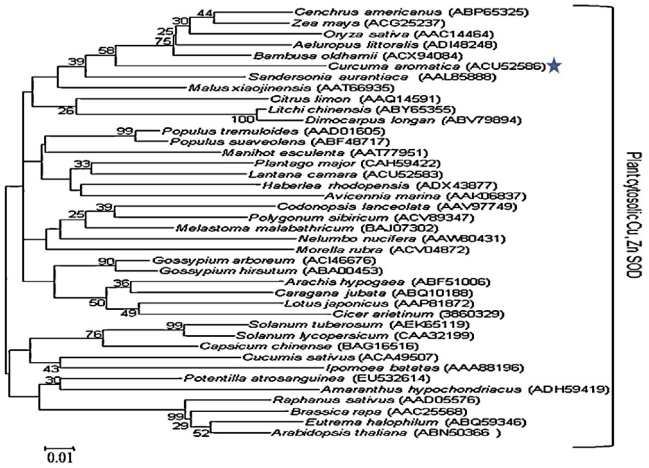

Fig. 2. Phylogenetic relationships of Ca–Cu,Zn SOD with plant Cu,Zn SOD sequences retrieved from NCBI database. Evolutionary history was inferred by the neighbor-joining method using MEGA5 software. The scale bar represents 5% dissimilarity between amino acid positions. GeneBank accession numbers are given in parentheses. Star (⋆) sign represent the position of Ca–Cu,Zn SOD in the phylogenetic tree.

Phylogenetic analysis showed that the clade *C. aromatica* (Family: Zingiberaceae) was close to *B. oldhamii* (Family: Poaceae) and *Sandersonia aurantiaca* (Family: Colchicaceae) (Fig. 2).

3.2. Kinetic parameters of Ca–Cu,Zn SOD

Ca–Cu,Zn SOD was a protein of 17.5 kDa (Fig. 3), as expected based on its amino acid composition. Different concentrations of riboflavin (0.0625–0.75 μM) were used to determine kinetic parameters of Ca–Cu,Zn SOD. The enzyme exhibited saturation at riboflavin concentration of 0.25 μM and above (Fig. 4a). Lineweaver–Burke plots revealed a linear relationship as evident from R^2 values of 0.9266. The K_m and V_{max} values were 0.047 ± 0.008 μM and 1250 ± 24 units/mg of protein, respectively (Fig. 4b).

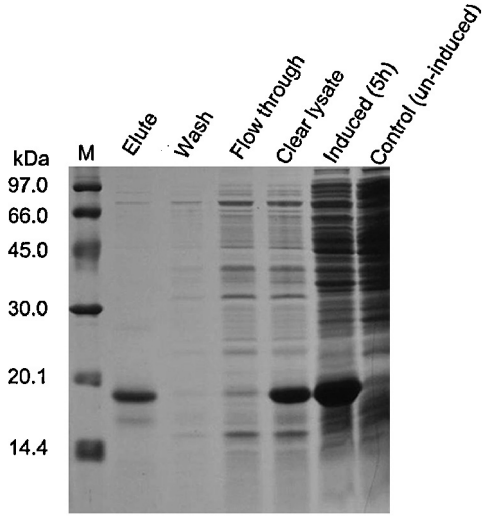

Fig. 3. Purification of Ca–Cu,Zn SOD expressed in *E. coli* using Ni-NTA agarose under native conditions. Protein was visualized by silver staining. M, molecular weight marker (Amersham, UK).

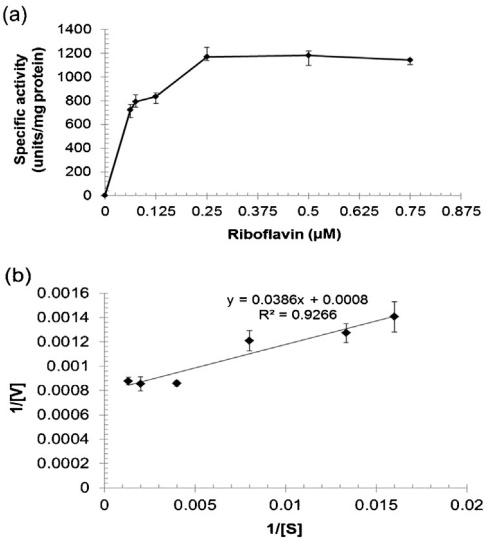

Fig. 4. Michaelis–Menten (a) and Lineweaver–Burk (b) plots of Ca–Cu,Zn SOD. K_m and V_{max} were calculated as described in Section 2.

3.3. Effect of temperature and pH on Ca–Cu,Zn SOD activity

Maximum enzyme activity was observed at 20 °C (Fig. 5a and b) and the activity declined at other temperatures studied. Ca–Cu,Zn SOD retained partial activity even after autoclaving, but as a function of assay temperature. Autoclaved Ca–Cu,Zn SOD exhibited 40% of maximum activity of un-autoclaved enzyme at 20 and 30 °C. A gradual decline of activity was observed at higher assay temperatures of 40–80 °C (Fig. 5b). Interestingly, autoclaved SOD showed 50% of maximum activity of un-autoclaved enzyme at 4 and 10 °C followed by a sharp decline in activity at "0" and sub-zero temperature of −10 °C.

SOD was functional at a pH range of 6.0–9.0 with highest activity observed at pH 7.8 (Fig. 5c). Ca–Cu,Zn SOD was stable for 2 h at pH of 3.0–9.0 (Fig. 5d). SOD activity at pH 10.0 dropped down by 23.08 ± 4.96% of the maximum activity after 2 h of incubation. At 24 h of incubation, the enzyme retained more than 80% activity in the pH range of 3.0–9.0, whereas at pH 10.0 the enzyme lost 36.21 ± 6.91% of the maximum activity.

3.4. Effect of denaturant, reductants and inhibitors of SOD

Activity of Ca–Cu,Zn SOD decreased with increasing concentration of GuHCl, wherein 2 M GuHCl exhibited 60.80 ± 3.26% of the maximum activity (Fig. 6a). Increasing the GuHCl concentration to 5 M resulted in 84.58 ± 3.56% loss of activity. Ca–Cu,Zn SOD exhibited remarkable resistance to reducing agents wherein 87.47 ± 0.68% and 83.06 ± 0.28% of the activity was observed at 2.5 mM of DTT and 3 mM of 2-ME, respectively (Fig. 6b). Similarly, addition of EDTA, a potential inhibitor of Cu,Zn SOD, inhibited the SOD activity, but at higher concentration (Fig. 6b). Ca–Cu,Zn SOD retained 85.84 ± 2.13% activity upto 0.5 mM of EDTA and thereafter showed decrease in activity. Increasing concentration of H_2O_2 also inhibited SOD activity and the enzyme retained 42.99 ± 2.57% of the maximum activity at 2 mM concentration (Fig. 6b).

3.5. Effect of incubation at 80 °C on Ca–Cu,Zn SOD

Ca–Cu,Zn SOD exhibited 30.84 ± 1.16% of the maximum activity after heating for 180 min at 80 °C (Fig. 7). No latency period was observed for thermal inactivation. Thermal inactivation exhibited linear relationship for zero, first, and second order thermal inactivation kinetics and the corresponding correlation coefficient

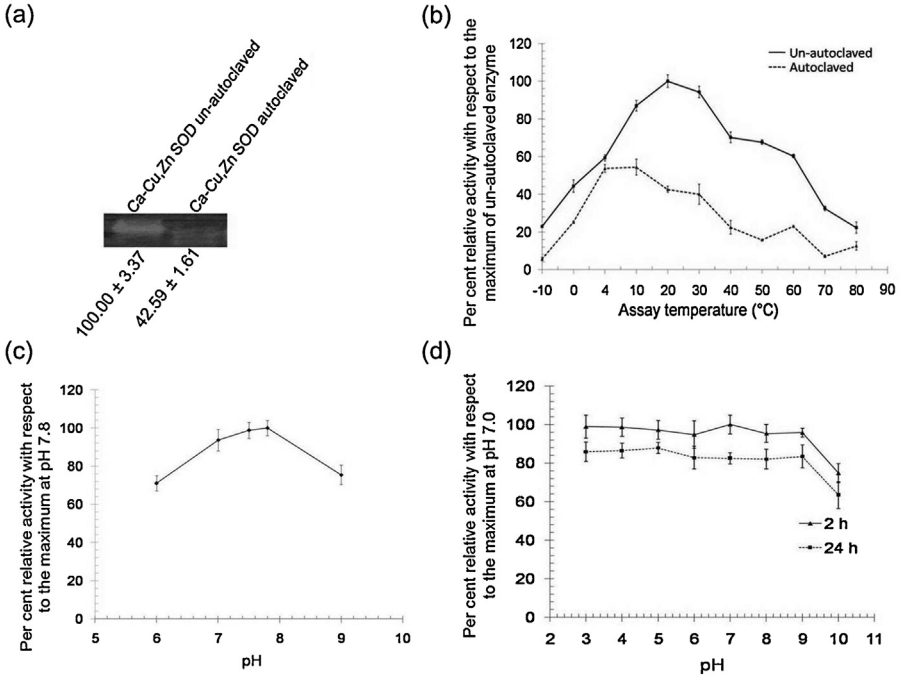

Fig. 5. Effect of autoclaving (a), assay temperature (b), pH (c) and pH of storage buffer and storage duration (d) on Ca–Cu,Zn SOD activity. Panel "a" shows activity staining gel in which equal quantity (300 ng) of Ca–Cu,Zn SOD was used and per cent relative activities are shown at the bottom of the panel. V_{max} of Ca–Cu,Zn SOD was 1250 ± 24 units/mg of protein. Values were mean ± SE of three separate replicates.

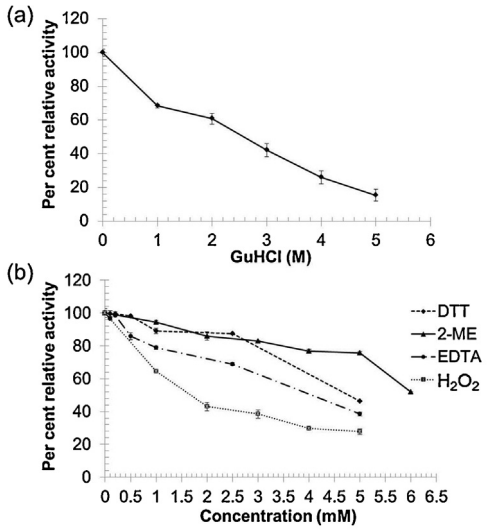

Fig. 6. Effect of various treatments on the activity of Ca–Cu,Zn SOD. Percent relative activity is activity with respect to the maximum enzyme activity of un-treated control. Values were mean ± SE of three separate replicates.

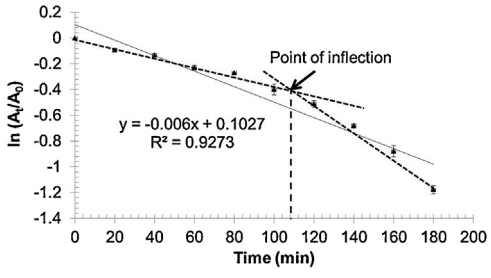

Fig. 7. Thermal inactivation kinetics of Ca–Cu,Zn SOD. Values were mean ± SE of three separate replicates. A_t, residual activity that remains after heating the enzyme for time t; A_0, initial enzyme activity before heating. Point of inflection was defined as "time point at which there was sudden decline in the enzyme activity".

(r) values were −0.989, −0.959, and 0.953, respectively. Kinetic parameters were calculated based on first-order thermal inactivation kinetics. Thermal inactivation rate constant (k_d) and half-life of thermal inactivation ($t_{1/2}$) calculated for first-order thermal inactivation kinetics at 80 °C were $6.54 \pm 0.17 \times 10^{-3}$ min^{-1} and 106.07 ± 2.68 min, respectively (Fig. 7). It was observed that thermal inactivation trend at 80 °C followed a linear trend up to 110 min (as shown by dotted line) and thereafter there was a sudden decline of activity. This point was defined as point of inflection and is represented by an arrow mark.

3.6. Measurements of protein stability by thermal unfolding

The heat-induced unfolding of Ca–Cu,Zn SOD produced a DSC profile that consisted of a single endothermic transition under the experimental conditions. Accordingly, T_m of purified Ca–Cu,Zn SOD was found to be 70.45 °C with enthalpy change (ΔH) of 1.853E4 kcal/mol/°C for protein unfolding process (Fig. 8).

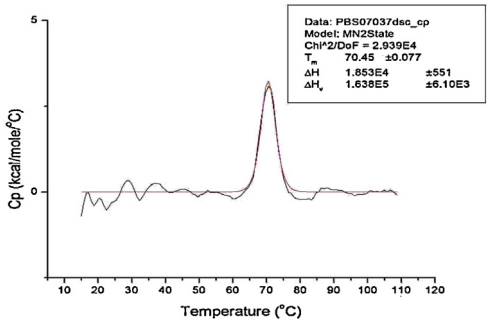

Fig. 8. Differential scanning calorimetry scan of Ca–Cu,Zn SOD in sodium phosphate buffer (100 mM, pH 7.4). C_p, heat capacity; ΔH, enthalpy change; ΔH_v, van't Hoff enthalpy change; T_m, midpoint of thermal transition.

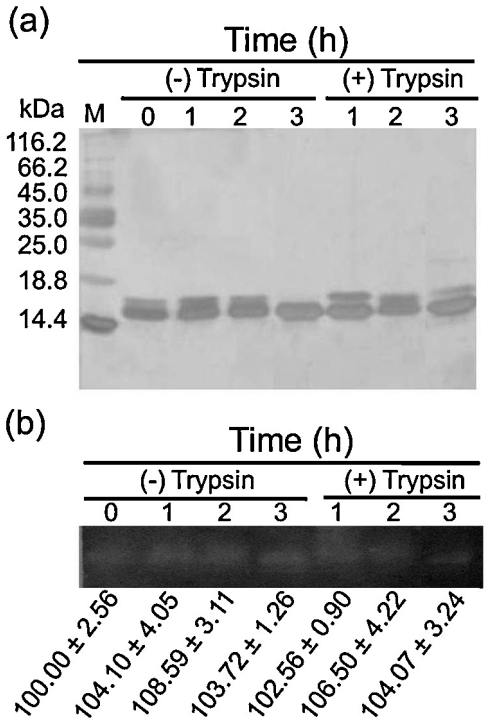

Fig. 9. Effect of trypsin on Ca–Cu,Zn SOD. Panel "a" shows the SDS-PAGE analysis using 1 μg of Ca–Cu,Zn SOD. M, molecular weight marker (Fermentas, USA). Gel for SOD activity is shown in panel "b". Values on lower side of the panel are percent relative activities of SOD with respect to 0 h control. Values were mean ± SE of three separate replicates.

3.7. Resistance of Ca–Cu,Zn SOD to cleavage by trypsin

Putative trypsin cleavage sites were obtained at positions 2, 23, 35, 58, 88, 98, 121, 134, 147, 154, and 162 as analyzed by PeptideCutter cutter software. However, Ca–Cu,Zn SOD was resistant to proteolytic cleavage by trypsin, as evident from intact bands in SDS-PAGE analysis (Fig. 9a) and also revealed by no loss of activity in activity stained gel (Fig. 9b).

3.8. Resistance to SDS-binding of Ca–Cu,Zn SOD

Boiled protein migrated to monomeric position whereas unboiled protein was visualized at dimeric position (Fig. 10) suggesting resistance of Ca–Cu,Zn SOD to SDS binding or SDS-mediated denaturation.

4. Discussion

Superoxide dismutase protects aerobic organisms from ROS mediated toxic effects by dismutating $O_2^{-\bullet}$ to O_2 and H_2O_2 [7–9]. Owing to its antioxidant property, SOD is indispensable for aerobic organisms, and has enormous applications in human health, food and pharmaceutical industries. Industrial applications would demand kinetically stable enzyme. This study described a kinetically stable Cu,Zn SOD from *C. aromatica*. Ca–Cu,Zn SOD had putative functional/conserved domains and secondary structures (Fig. 1a and b), which were essential to render characteristic functionality to the enzyme. Alignment of deduced amino acid sequences with the corresponding sequences available at gene databank revealed the presence of conserved amino acid residues important in co-ordinating Cu^{2+} and Zn^{2+} in Ca–Cu,Zn SOD (Supplementary Fig. 4). Cu^{2+} ion is required for oxidation–reduction reactions and is important in providing functionality to the enzyme, whereas Zn^{2+} ion is (i) needed for structural stability of the enzyme

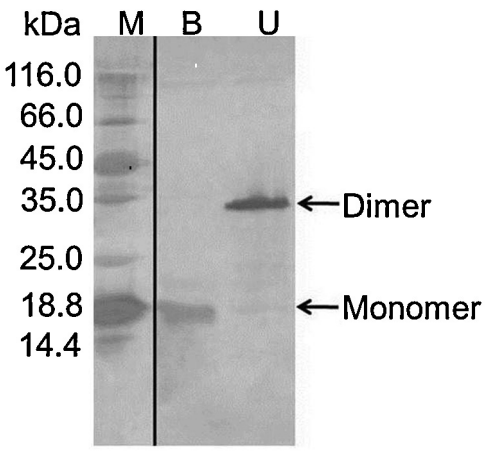

Fig. 10. Effect of boiling on Ca–Cu,Zn SOD in the presence of SDS. U, unboiled; B, boiled for 10 min immediately prior to loading onto the 15% SDS-PAGE in the presence (+) of SDS. 2-ME was omitted (−) from the sample loading buffer in both. M, molecular weight marker (Fermentas, USA).

[34], (ii) essential for the dissociation of the H_2O_2, and (iii) important for the pH stability of the reaction [35]. In the oxidized form, Cu^{2+} ion is coordinated by the nitrogen atoms of four histidine residues; Zn^{2+} ion is coordinated by three histidines and one aspartic acid residue. The two metal ions are simultaneously coordinated by a single histidine (His-62) residue (termed the "histidine bridge" or the "bridging imidazolate") in a structural motif so far found only in Cu,Zn SODs. In the absence of coordinated Cu^{2+} and Zn^{2+} ions, the β-barrel and dimer interface of Cu,Zn SOD remained intact, but the metal binding loops were disordered. The 3-D model of Ca–Cu,Zn SOD suggested the protein to exist as a dimer (Fig. 1d).

Two cysteines (Cys-56 and Cys-145) that form a disulfide bond were conserved in Ca–Cu,Zn SOD as is reported in other Cu,Zn SOD sequences [36]. Metal ion coordination and disulfide formation promote homodimerization of Cu,Zn SOD subunits [37] and are linked to conformational stability of Cu,Zn SODs. In bovine Cu,Zn SOD, Zn^{2+} ion stoichiometry played an important role in the oxidative refolding of SOD by accelerating the oxidative refolding, suppressing the aggregation during refolding, and helped the protein to form a compact structure whereas Cu^{2+} ion did not show significant effects [34].

Conserved domain analysis of Ca–Cu,Zn SOD showed the presence of Cu,Zn SOD signature 1 and signature 2 (Supplementary Fig. 4). These were reported from Cu,Zn SOD from *Avicennia marina* [35] and *Polygonum sibiricum* [38] as well. Ca–Cu,Zn SOD did not have any transmembrane domain which is suggestive of a cytosolic enzyme.

Ca–Cu,Zn SOD exhibited K_m and V_{max} values of 0.047 ± 0.008 μM and 1250 ± 24 units/mg of protein (Fig. 4a and b). K_m is a constant characteristic of each enzyme that reflects the affinity of enzyme toward its substrate. These values can be used to discriminate the enzyme isoforms from different organisms or tissues. For example, Cu,Zn SOD of *Cicer arietinum* had K_m value of 10.16 ± 2.5 μM [39], which is much higher to that of Ca–Cu,Zn SOD. Since *in vivo* substrate levels usually are too low for enzyme activities to reach maximum velocities, reaction velocities are strongly affected by enzyme-substrate affinity. Lower K_m value of Ca–Cu,Zn SOD suggests higher affinity to substrate even at very low concentrations and therefore, high catalytic rate of superoxide dismutation. Likewise, different V_{max} values were reported for Cu,Zn SOD from different sources [29,39].

Interestingly, the enzyme tolerated autoclaving to certain extent and also exhibited activity over a wide temperature range (Fig. 5a and b). Such results were unique for Ca–Cu,Zn SOD and has been

reported at least for Cu,Zn SOD of *Potentilla atrosanguinea* (Family: Rosaceae) [9,17]. Though phylogenetic analysis revealed that the clades of *P. atrosanguinea* and *C. aromatica* were distant from each other and the later showed close relatedness with *B. oldhamii* (Family: Poaceae) and *S. aurantiaca* (Family: Colchicaceae) (Fig. 2). Data suggested that overall folded structure of the enzyme governed the trait of autoclave stable behavior of the enzyme not the phylogenetic relatedness. Further, DSC provides information on the thermal stability of a protein under different solvent conditions, and also provides information on the solubility of the unfolded forms of the protein. Since Ca–Cu,Zn SODs protein had higher T_m value (Fig. 8) as compared to other reported SODs suggesting it to be relatively thermostable protein [40].

Ca–Cu,Zn SODs was functional at a pH range of 6.0–9.0 with maximum activity observed at pH 7.0–8.0. The catalytic activity of Cu,Zn SODs decreased at pH 6.0 and 9.0 (Fig. 4c). The activity of Cu,Zn SODS is generally considered as being pH-independent in the range 5.0–9.0. The activity of Cu,Zn SODs is dependent on ionic strength and alkaline pH in a way that typically reflects the functional role of charged amino acid residues, in particular arginine and lysine.

Inhibition of Cu,Zn SODs at alkaline pH might be due to deprotonation of basic residues near the active site of the enzyme. At higher pH, loss of positive charge (removal of H^+) on the surface and in the active center of SOD affects the availability of $O_2^{-\bullet}$ to the active site and would lead to decreased SOD activity. Ca–Cu,Zn SOD had 10 positively charged residues (seven lysine and three arginine residues). These amino acids are distributed on the surface as well as on the active site of Cu,Zn SOD. Positive charge on the surface and in the active site, in combination with the electrostatic repulsive effect of the negatively charged residues, guides the anionic substrate $O_2^{-\bullet}$ to the active site of the enzyme [41]. Decrease in the enzyme activity at pH 6.0 (Fig. 5c) might be due to net negative charge on the protein surface leading to electrostatic repulsive effects to $O_2^{-\bullet}$. Lowering of pH might cause electrostatic repulsive effect to $O_2^{-\bullet}$ and affect availability of substrate to active site.

An attempt was also made to study the impact of storage pH on the activity of Ca–Cu,Zn SOD. Ca–Cu,Zn SODs retained >70% of maximum activity over a pH range of 5.0–9.0 for 2 h (Fig. 5d). Further decrease in activity was observed at 24 h of storage at pH 3.0, 4.0, 9.0 and 10.0. The results were consistent with Cu,Zn SOD from other sources [42]. The effect of pH storage on stability of Ca–Cu,Zn SOD under study was better than that of Cu,Zn SOD purified from *Withania somnifera* (enzyme was stable in broad pH range from 2.5 to 8.0, but activity decreased above pH 8.0 after 1 h of storage at 32 ± 2 °C) [43], *Aerobacter aerogenesis* (enzyme was comparatively stable at pH 7.0–11.0, but was rapidly inactivated below pH 7.0 after 36 h of storage) [44] and chicken erythrocytes (enzyme was stable at pH range of 6.0–9.0 with decline in activity at pH 10.0, after 2 h of storage at 25 °C) [45].

Cu,Zn SODs are generally resistant to denaturating agents, heating and chemical treatments. Ca–Cu,Zn SOD was fairly resistant to denaturation by GuHCl, tolerated high concentrations of reducing agents 2-ME, DTT, and exhibited activity in the presence of higher concentrations of EDTA and H_2O_2 (Fig. 6a and b). The remarkably high resistance to reducing agents 2-ME and DTT suggests the fairly stable disulfide bridge. EDTA is a common chelating agent, which affects the enzyme activity by chelating the Cu^{2+} ion. H_2O_2 inactivates Cu,Zn SODs by destroying the His ligands of Cu and Zn in the protein [46]. Therefore, apparent resistance of Ca–Cu,Zn SODs to these agents might be due to conformational lock of the enzyme to protect His ligands and other amino acids important in maintaining the catalytic active site including disulfide bonds.

Ca–Cu,Zn SOD exhibited fairly high level of resistance to heat denaturation at 80 °C (Fig. 7). During thermal inactivation kinetics an inflection point was observed that may be considered as a point where activity started declining due to conversion of comparatively more active dimeric form to less active monomeric form. Cu,Zn SODs from various sources showed varied level of resistance to heat denaturation *e.g.* Cu,Zn SODs from *Radix lithospermi* and *Anas platyrhynchos domestica* exhibited irreversible heat inactivation at 60 °C and 70 °C, respectively [41,47], whereas Cu,Zn SOD from *P. atrosanguinea* [9] and *W. somnifera* [43] exhibited very high resistance to thermal inactivation at 80 °C. These differences in thermostability among species suggest that amino acid sequences influence structural organization of SODs, wherein various interactions including hydrophobic interactions, dimer interface contacts, and disulfide bridges play a critical role [9]. Cleavage of dimer interface contact areas by dissociation of the subunits, with destruction of the active centers, might be considered as one of the reasons of loss of enzyme activity upon heat incubation for long periods of times [48].

Resistance of the enzyme to limited proteolytic cleavage and resistance to SDS-binding are considered as important parameters of kinetic stability of the protein [32,49]. Kinetic stability is a property of proteins that are trapped in their native conformations by an energy barrier and as a result are resistant to unfolding, presumably to protect against aggregation or premature degradation [32]. High specific activity, resistance to heat denaturation, resistance to proteases, and activity at a wide pH range are some of the indicators of kinetically stable and industrially relevant enzymes [50].

Trypsin cleaves the protein next to Lys and Arg residues in the polypeptide backbone [51]. Though Ca–Cu,Zn SOD had potential trypsin cleavage sites, our results on limited trypsin proteolysis showed intact protein bands on SDS-PAGE (Fig. 9a). Also, no loss of enzymatic activity was observed on activity stained gel (Fig. 9b), suggesting the protein to have a global confirmation that avoid the proteolytic action. Cu,Zn SODs generally have a short plasma half-life (6–15 min) and precludes it for application as a therapeutic protein for human application [7]. Proteolysis is considered as one of the common causes of protein instability in serum plasma [52]. Ca–Cu,Zn SOD exhibiting resistance to limited trypsin proteolysis can therefore be used as a therapeutic protein.

SDS is known to denature proteins by irreversibly trapping the proteins in transiently or partially unfolded states. Decreased rate of local and global unfolding of kinetically stable proteins accounts for their resistance to SDS-induced denaturation [53]. Ca–Cu,Zn SODs showed resistance to SDS-binding since unboiled protein appeared as dimer (Fig. 10), suggesting it to be a kinetically stable protein.

To conclude, the present work identified a kinetically stable *Cu,Zn SOD* from *C. aromatica*, which exhibited catalytic activity across wide temperature and pH ranges, retained partial activity after autoclaving, resisted cleavage by proteolytic enzyme trypsin, tolerated varying concentrations of a denaturating agent, reductants, inhibitors and was fairly resistant to inactivation at 80 °C for 180 min and had a T_m of 70.45 °C. Kinetic stability of proteins is an important property for adaptation and survival under the harsh environments and hence the identified gene has implications in raising the transgenic plants for the stress-full environment where production of $O_2^{-\bullet}$ is inevitable and its scavenging is a necessity to avoid any damage to organism [54,55]. Since the enzyme is a kinetically stable moiety, the enzyme will find industrial applications wherein $O_2^{-\bullet}$ production is inevitable and the scavenging is desirable [7,8].

Acknowledgements

Authors thank Council of Scientific and Industrial Research (CSIR) for funding through project “Plant Diversity: Studying adaptation biology and understanding/exploiting medicinally

important plants for useful bioactives (SIMPLE)-BSC0109". The authors AK, AK and SB gratefully acknowledge CSIR, New Delhi, India for Research fellowships. Manuscript represents IHBT communication number 3594.

Appendix A. Supplementary data

Supplementary data associated with this article can be found, in the online version, at doi:10.1016/j.procbio.2014.04.010.

References

[1] Apel K, Hirt H. Reactive oxygen species: metabolism, oxidative stress, and signal transduction. Annu Rev Plant Biol 2004;55:373–99.
[2] Suzuki N, Mittler R. Reactive oxygen species and temperature stresses: a delicate balance between signaling and destruction. Physiol Plantarum 2006;126:45–51.
[3] Karuppanapandian T, Moon JC, Kim C, Manoharan K, Kim W. Reactive oxygen species in plants: their generation, signal transduction, and scavenging mechanisms. Aust J Crop Sci 2011;5:709–25.
[4] Sharma P, Jha AB, Dubey RS, Pessarakli M. Reactive oxygen species, oxidative damage, and antioxidative defense mechanism in plants under stressful conditions. J Bot 2012;217037:1–26.
[5] García Echauri SA, Gidekel M, Gutierrez Moraga A, Ordóñez L, Rojas G, Contreras JA, et al. Heterologous expression of a novel psychrophilic Cu/Zn superoxide dismutase from *Deschampsia Antarctica*. Process Biochem 2009;44:969–74.
[6] Foyer CH, Noctor G. Redox regulation in photosynthetic organisms: signaling, acclimation, and practical implications. Antioxid Redox Signal 2009;11:861–905.
[7] Bafana A, Dutt S, Kumar A, Kumar S, Ahuja PS. Basic and applied aspects of superoxide dismutase. J Mol Catal B: Enzymatic 2011;68:129–38.
[8] Bafana A, Dutt S, Kumar S, Ahuja PS. Superoxide dismutase: an industrial perspective. Crit Rev Biotechnol 2011;31:65–76.
[9] Kumar A, Dutt S, Bagler G, Ahuja PS, Kumar S. Engineering a thermo-stable superoxide dismutase functional at sub-zero to >50 °C, which also tolerates autoclaving. Sci Rep 2012;2:387, http://dx.doi.org/10.1038/srep00387.
[10] Auclair JR, Brodkin HR, D'Aquino JA, Petsko GA, Ringe D, Agar JN. Structural consequences of cysteinylation of Cu/Zn-superoxide dismutase. Biochemistry 2013;52:6145–50.
[11] Alscher RG, Erturk N, Heath LS. Role of superoxide dismutases (SODs) in controlling oxidative stress in plants. J Exp Bot 2002;53:1331–41.
[12] Youn HD, Kim EJ, Roe JH, Hah YC, Kang SO. A novel nickel-containing superoxide dismutase from *Streptomyces* spp. Biochem J 1996;318:889–96.
[13] Abreu IA, Cabelli DE. Superoxide dismutases—a review of the metal-associated mechanistic variations. Biochim Biophys Acta 2010;1804:263–74.
[14] Kumar S, Sahoo R, Ahuja, PS. A novel isozyme of autoclavable SOD: a process for the identification and extraction of the SOD and use of the said SOD in the cosmetic, food and pharmaceutical composition. US Patents. US 6,485,950 [26.11.2002].
[15] Kumar S, Sahoo R, Ahuja PS. A novel isozyme of autoclavable SOD: a process for the identification and extraction of the SOD and use of the said SOD in the cosmetic, food and pharmaceutical composition. US Patent. US 7,037,697 B2 [02.05.2006].
[16] Yogavel M, Mishra PC, Gill J, Bhardwaj PK, Dutt S, Kumar S, et al. Structure of a superoxide dismutase and implications for copper-ion chelation. Acta Crystallogr D Biol Crystallogr 2008;64:892–901.
[17] Bhardwaj PK, Sahoo R, Kumar S, Ahuja PS. A gene encoding autoclavable superoxide dismutase and its expression in *E. coli*. US patent. US 7,888,088 B2 [15.02.2011].
[18] Li RK, Fu CL, Chen P, Ng TB, Ye XY. High-level expression of a sika dear (*Cervus Nippon*) Cu/Zn superoxide dismutase in *Pichia pastoris* and its characterization. Environ Toxicol Pharmacol 2013;35:185–92.
[19] Pant N, Misra H, Jain DC. Phytochemical investigation of ethyl acetate extract from *Curcuma aromatica* Salisb rhizomes. Arab J Chem 2013;6:279–83.
[20] Hong JY, Sato EF, Kira Y, Nishikawa M, Shimada K, Inoue M. Curcuma aromatica inhibits diabetic nephropathy in the rat. J Food Sci 2006;71:S626–32.
[21] Srividya AR, Dhanabal P, Bavadia P, Vishnuvarthan VJ, Kumar MNS. Antioxidant and antidiabetic activity of *Curcuma aromatica*. Int J Res Ayurveda Pharma 2012;3:401–5.
[22] Gill SS, Tuteja N. Reactive oxygen species and antioxidant machinery in abiotic stress tolerance in crop plants. Plant Physiol Biochem 2010;48:909–30.
[23] Ghawana S, Paul A, Kumar H, Kumar A, Singh H, Bhardwaj PK, et al. An RNA isolation system for plant tissues rich in secondary metabolites. BMC Res Notes 2011;4:85.
[24] Benkert P, Schwede T, Tosatto SC. QMEANclust: estimation of protein model quality by combining a composite scoring function with structural density information. BMC Struct Biol 2009;9:35.
[25] Benkert P, Biasini M, Schwede T. Toward the estimation of the absolute quality of individual protein structure models. Bioinformatics 2011;27:343–50.
[26] Tamura K, Peterson D, Peterson N, Stecher G, Nei M, Kumar S. MEGA5: molecular evolutionary genetics analysis using maximum likelihood, evolutionary distance, and maximum parsimony methods. Mol Biol Evol 2011;28:2731–9.
[27] Chevallet M, Luche S, Rabilloud T. Silver staining of proteins in polyacrylamide gels. Nat Protoc 2006;1:1852–8.
[28] Vyas D, Kumar S, Ahuja PS. Tea (*Camellia sinensis*) clones with shorter periods of winter dormancy exhibit lower accumulation of reactive oxygen species. Tree Physiol 2007;27:1253–9.
[29] Niyomploy P, Boonsombat R, Karnchanatat A, Sangvanich P. A superoxide dismutase purified from the roots from *Stemona tuberosa*. Prep Biochem Biotechnol 2013, http://dx.doi.org/10.1080/10826068.2013.868356.
[30] Bian Y, Rong Z, Chang TMS. Polyhemoglobin-superoxide dismutase-catalase-carbonic anhydrase: a novel biotechnology-based blood substitute that transports both oxygen and carbon dioxide and also acts as an antioxidant. Artif Cells Blood Substit Immobil Biotechnol 2011;39:127–36.
[31] Kishore D, Kundu S, Kayastha AM. Thermal, chemical and pH induced denaturation of a multimeric β-galactosidase reveals multiple unfolding pathways. PLoS ONE 2012;7:e50380.
[32] Manning M, Colon W. Structural basis of protein kinetic stability: resistance to sodium dodecyl sulfate suggests a central role for rigidity and a bias toward beta-sheet structure. Biochemistry 2004;43:11248–54.
[33] de Beus MD, Chung J, Colón W. Modification of cysteine 111 in Cu/Zn superoxide dismutase results in altered spectroscopic and biophysical properties. Protein Sci 2004;13:1347–55.
[34] Li HT, Jiao M, Chen J, Liang Y. Roles of zinc and copper in modulating the oxidative refolding of bovine copper, zinc superoxide dismutase. Acta Biochim Biophys Sin (Shanghai) 2010;42:183–94.
[35] Jabeen U, Salim A, Abbas A. Prediction of post translational modifications in *Avicennia marina* Cu–Zn superoxide dismutase: implication of Glycation on the Enzyme Structure. J Chem Soc Pak 2012;34:404–14.
[36] Petersen SV, Valnickova Z, Oury TD, Crapo JD, Chr Nielsen N, Enghild JJ. The subunit composition of human extracellular superoxide dismutase (EC-SOD) regulates enzymatic activity. BMC Biochem 2007;8:19.
[37] Naiki H, Higuchi K, Hosokawa M, Takeda T. Fluorometric determination of amyloid fibrils in vitro using the fluorescent dye thioflavin T1. Anal Biochem 1989;177:244–9.
[38] Qu CP, Xu ZR, Liu GJ, Liu C, Li Y, Wei ZG, et al. Differential expression of copper-zinc superoxide dismutase gene of *Polygonum sibiricum* leaves, stems and underground stems, subjected to high-salt stress. Int J Mol Sci 2010;11:5234–45.
[39] Singh S, Singh AN, Verma A, Dubey VK. A novel superoxide dismutase from *Cicer arietinum* L. seedlings: isolation, purification and characterization. Protein Pept Lett 2013;20:741–8.
[40] Rodriguez JA, Shaw BF, Durazo A, Sohn SH, Doucette PA, Nersissian AM, et al. Destabilization of apoprotein is insufficient to explain Cu,Zn-superoxide dismutase-linked ALS pathogenesis. Proc Natl Acad Sci USA 2005;102:10516–21.
[41] Haddad NIA, Yuan QS. Purification and some properties of Cu,Zn superoxide dismutase from *Radix lethospermi* seed, kind of Chinese traditional medicine. J Chromatogr B: Anal Technol Biomed Life Sci 2005;818:123–31.
[42] Wang X, Yang H, Ruan L, Liu X, Li F, Xu X. Cloning and characterization of a thermostable superoxide dismutase from the thermophilic bacterium Rhodothermus sp. XMH10. J Ind Microbiol Biotechnol 2008;35:133–9.
[43] Madanala R, Gupta V, Deeba F, Upadhyay SK, Pandey V, Singh PK, et al. A highly stable Cu/Zn superoxide dismutase from *Withania somnifera* plant: gene cloning, expression and characterization of the recombinant protein. Biotechnol Lett 2011;33:2057–63.
[44] Kim SW, Lee SO, Lee TH. Purification and characterization of superoxide dismutase from *Aerobacter aerogenes*. Agric Biol Chem 1991;55:101–8.
[45] Aydemir T, Tarhan L. Purification and partial characterisation of superoxide dismutase from chicken erythrocytes. Turk J Chem 2001;25:451–9.
[46] Bueno P, Varela J, Gimenez-Gallego G, del Rio LA. Peroxisomal copper, zinc superoxide dismutase (characterization of the isoenzyme from watermelon cotyledons). Plant Physiol 1995;108:1151–60.
[47] Liu W, Zhu RH, Li GP. Wang DC. cDNA cloning, high-level expression, purification, and characterization of an avian Cu,Zn superoxide dismutase from Peking duck. Protein Express Purif 2002;25:379–88.
[48] Hong J, Moosavi-Movahedi AA, Ghourchian H, Amani M, Amanlou M, Chilaka FC. Thermal dissociation and conformational lock of superoxide dismutase. J Biochem Mol Biol 2005;38:533–8.
[49] Sanchez-Ruiz JM. Protein kinetic stability. Biophys Chem 2010;148:1–15.
[50] Daniel RM, Toogood HS, Bergquist PL. Thermostable proteases. Biotechnol Genet Eng Rev 1996;13:51–100.
[51] Rodriguez J, Gupta N, Smith RD, Pevzner PA. Does trypsin cut before proline. J Proteome Res 2008;7:300–5.
[52] Kotzia GA, Lappa K, Labrou NE. Tailoring structure–function properties of L-asparaginase: engineering resistance to trypsin cleavage. Biochem J 2007;404:337–43.
[53] Xia K, Zhang S, Solina BA, Barquera B, Colon W. Do prokaryotes have more kinetically stable proteins than eukaryotic organisms. Biochemistry 2010;49:7239–41.
[54] Gill T, Sreenivasulu Y, Kumar S, Ahuja PS. Over-expression of Potentilla superoxide dismutase improves salt stress tolerance during germination and growth in *Arabidopsis thaliana*. J Plant Genet Transgen 2010;1:1–10.
[55] Pal AK, Acharya K, Vats SK, Kumar S, Ahuja PS. Over-expression of PaSOD in transgenic potato enhances photosynthetic performance under drought. Biol Plant 2012;57:359–64.